Electromagnetic Performance Analysis of Flux-Switching Permanent Magnet Tubular Machine with Hybrid Cores

Shaopeng Wang, Chengcheng Liu, Youhua Wang, Gang Lei, Youguang Guo, and Jianguo Zhu

***Abstract*—The performance of traditional flux switching permanent magnet tubular machine (FSPMTM) are improved by using new material and structure in this paper. The existing silicon steel sheet making for all mover cores or part of stator cores are replaced by soft magnetic composite (SMC) cores, and the lamination direction of the silicon steel sheet in stator cores have be changed. The eddy current loss of the machine with hybrid cores will be reduced greatly as the magnetic flux will not pass through the silicon steel sheet vertically. In order to reduce the influence of end effect, the unequal stator width design method is proposed. With the new design, the symmetry of the permanent magnet flux linkage has been improved greatly and the cogging force caused by the end effect has been reduced. Both 2-D and 3-D finite element methods (FEM) are applied for the quantitative analysis.**

***Index Terms*—Flux switching permanent magnet tubular machine, soft magnetic composite (SMC), hybrid cores, unequal width stator, finite element method (FEM).**

I. INTRODUCTION

NOWDAYS, there is a trend to use linear machine for replacing rotary machine in linear driving applications, as linear machine can have higher force density and efficiency [1]-[5]. Among various kind of linear machines, flux switching permanent magnet tubular machine (FSPMTM) draws a great interest from researchers for its robust structure, high drive force density and low material cost required [6]-[8]. However, in the traditional FSPMTM, the silicon steel sheet is stacked along the axis direction to form stator cores and mover cores, thus the magnetic flux passes through the silicon steel sheet vertically, which will result large eddy current loss [9]-[10]. In order to reduce the eddy current loss of silicon steel sheet, it has been validated that a partial slitting along redial direction is efficient. The method aims to further increasing in the eddy current path [11]. Meanwhile, new magnetic material is also used to replace silicon steel sheet to reduce eddy current loss.

Soft magnetic composite (SMC) materials with isotropy magnetic permeability solved the problem of magnetic flux is confined in 2D plane of silicon steel sheet. SMC material is made by the powder metallurgy technology, which mixes the iron powder and insulating layer with the organic material. However, traditional electrical machine made by SMC material has lower power density and higher hysteresis losses compared with that made by the silicon steel under low frequency operation. Furthermore, end effect is another negative factor for the FSPMTM, as it can not only increase the cogging force and force ripple but also bring the PM flux linkage waveform shifts toward to negative or positive direction which will make the machine easy for saturation [12]-[14].

In this paper, a new hybrid cores combined SMC material and silicon steel is proposed for FSPMTM， the direction of the stack of silicon steel will be changed to reduce the core loss. SMC material is a relatively new soft magnetic material, it has many special properties comparing with the traditional silicon steels, such as the magnetic and thermal isotropy, very low eddy current losses, etc. [15]. Since the silicon steel sheet and SMC material have different properties at different frequencies, the proportion of the silicon steel sheet and SMC material in the hybrid core needs to be analyzed as well.

In order to reduce the influence of the end effect on the cogging force, there are some methods in the existing research, such as modulating the machine, adding assistant teeth at the end, and adding skew poles [16]-[20]. In this paper, the unequal stator teeth method is proposed to decrease the end effect, by using this method the symmetry of the PM flux linkage can be improved and the cogging force and force ripple can be reduced. To show the advantage of adopted hybrid cores, the accurate core loss of FSPMTM is obtained using the 3-D rotational core loss calculation method, and the eddy current loss resulted by the flux path vertically through the silicon steel plane is included.

II. TOPOLOGY OF 3-D FSPMTM

Firstly, the FSPMTM with silicon steel cores (M1) and SMC

Manuscript was submitted for review on 25, April, 2019.

This work was supported in part by the National Natural Science Foundation of China under project 51877065 and Hebei Province Education Department Youth Talent Leading Project under grant BJ2018037, and in part by the State Key Laboratory of Reliability and Intelligence of Electrical Equipment under grant EERIKF2018005.

Shaopeng Wang, Chengcheng Liu, and Youhua Wang are with State Key Laboratory of Reliability and Intelligence of Electrical Equipment, Hebei University of Technology and Key Laboratory of Electromagnetic Field and Electrical Apparatus Reliability of Hebei Province, Hebei University of Technology, Tianjin, 300130, China (2016020@hebut.edu.cn, 522396000@qq.com, wangyi@hebut.edu.cn)

Gang Lei, and Youguang Guo are with the School of Electrical and Data Engineering, University of Technology Sydney, NSW 2007, Australia, (gang.lei@uts.edu.au, youguang.guo@uts.edu.au)

Jianguo Zhu is with school of electrical and information engineering, University of Sydeny, NSW 2007, Australia, (jianguo.zhu@sydney.edu.au)

Digital Object Identifier 10.30941/CESTEMS.2020.00007

cores (M2) are developed. For the silicon steel, the M19_29G is used and for SMC material the S360 from PMG Germany is used. As shown in Fig.1, the permanent magnets (PMs) in these two machines are located on the short primary stator side and they are magnetized along the axial direction. Adjacent PMs are magnetized along the opposite directions, and all the PMs are sandwiched between the U-shaped stator cores. The used winding is the global ring winding and it is located on the inner space of U shaped stator cores. In these FSPMTMs, there is no winding or PM on the long mover side, thus the material cost can be kept very low and the mechanical robustness can be guaranteed.

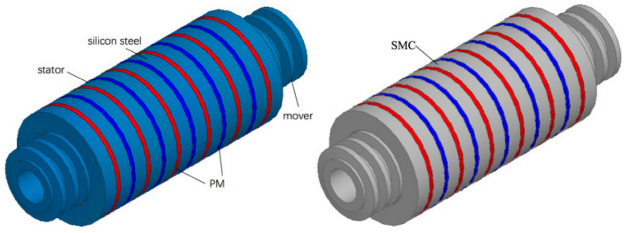

Fig. 1. Main topology of the FSPMTM, (a) M1, (b) M2.

Fig. 2 shows the main parameters of FSPMTFM. After the initial optimization, the main parameters of the proposed FSPMTM are obtained as tabulated in Table I.

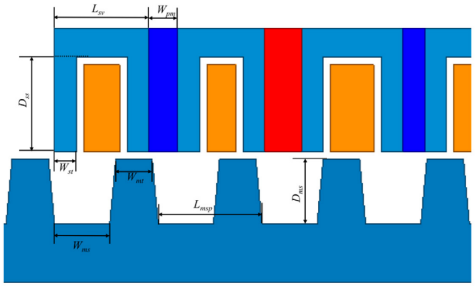

Fig. 2. Main parameter of FSPMTFM.

TABLE I
MAIN DIMENSIONS OF PROPOSED FSPMTM

Parameters	Symbol	Value	Unit
Stator inner radius	R_{si}	33	mm
Stator outer radius	R_{so}	50	mm
Stator yoke length	L_{sy}	13	mm
Stator slot depth	D_{ss}	7	mm
Stator tooth width	W_{st}	3	mm
PM width	W_{pm}	4	mm
Effective axial length	L_{ea}	200	mm
Air gap length	L_{ag}	1	mm
Shaft radius	R_{shaft}	15	mm
Mover outer radius	R_{mo}	32	mm
Mover slot depth	D_{ms}	9	mm
Mover slot width	W_{ms}	200/14-6.68	mm
Mover teeth width	W_{mt}	5	mm
Mover slot pitch length	L_{msp}	200/14	mm

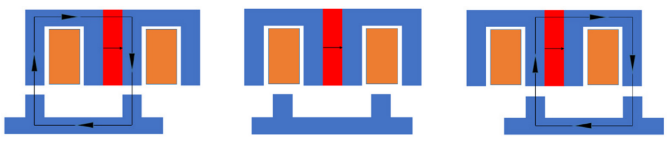

Fig. 3. Principle of flux switching.

Fig. 3 shows the basic flux switching operation principle. When the mover is aligned with the stator pole on the right side of PM, as shown in Fig. 3(a), it can be found that the flux flows out from the stator pole; it will produce a maximum positive flux linkage. As the mover continues to move to the position shown in figure 3(b), the flux linking the winding is almost zero cause the magnetic reluctance of the air of slot is very large, Then, the mover continues to move and aligns with the stator pole on the left side of PM, as shown in Fig. 3(c), and a maximum negative flux linkage is produced. As the mover moves, the ideal phase PM flux linkages, back EMF and armature current are shown in Fig. 4.

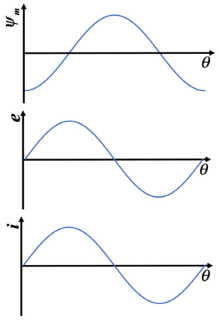

Fig. 4. Flux switching ideal waveform.

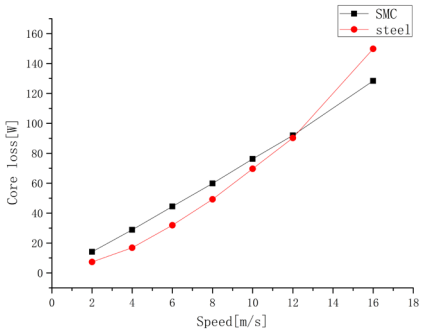

Fig. 5 Core loss of FSPMTM with M19_29G cores and SMC_s360 cores at different frequency.

In ideal situation, the additional eddy current loss is ignored, then the core loss comparison of FSPMTMs with different materials at the different mover speed is calculated, as shown in Fig. 5. As shown, 12 m/s is the boundary speed, the core loss of FSPMTM with SMC cores is lower than that with silicon steels when the speed is over than 12 m/s.

If the stator cores or mover cores are made by only using the silicon steels, then its magnetic flux will path through the silicon steel sheet plane vertically, and thus great eddy current loss will be resulted. As if only the SMC cores are applied, then its performance will be inferior to that with silicon steels at very low frequency. Therefore, the concept of hybrid cores with SMC material and silicon steels is proposed, where the direction of lamination has been changed as well.

When the lamination direction of silicon steel sheet is changed from axial direction to circumferential direction, the situation shown in Fig. 6(a) will be produced. The lamination of silicon steel sheet is not satisfactory and the air gap is extremely large. Thus, this lamination method is not good. Four tangential directions and parallel lamination of silicon steel sheets are selected as the lamination directions in this paper, as shown in Fig. 6(b). This lamination direction makes the relationship

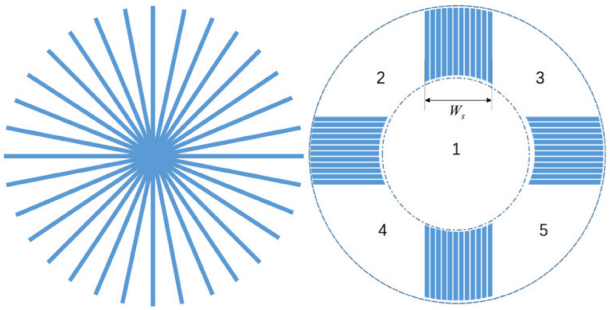

Fig. 6. Different direction of lamination of silicon steel sheet (a) The silicon steel sheet is laminated circumferentially (b) The silicon steel sheet is laminated along four tangential directions.

between the silicon steel sheets the same as that in the traditional lamination direction, and the air gap between the silicon steel sheets is small. For the magnetic flux path, the laminated direction shown in Fig. 6(b) enables the flux to flow completely in the plane of the silicon steel sheet rather than vertically across the stator yoke, thus the eddy current losses can be reduced greatly. It can be seen that in the four regions of the stacked silicon steel sheet, there are still five blank regions surrounded by dotted lines. The middle region 1 is the position of the mover, and the remaining 2、3、4 and 5 fan regions are considered as the stator parts made by using SMC materials. Where the lamination of silicon steel sheet is not satisfactory, SMC can be filled, which has three-dimensional magnetic properties to achieve magnetic conductivity, and does not produce a large number of eddy current loss. Similarly, the mover can be constructed in this way. It can be seen that such stacking method of silicon steel leaves a variable space, that is, the width W_s of silicon steel sheet in four tangential stacking ways. However, considering the stacking of silicon steel sheet and the consistency of SMC structure of the remaining four parts, the calculation in this paper maintains that W_s is equal. Moreover, considering the difficulty of lamination of silicon steel sheets, the variation range of W_s is no more than $2R_{si}$, which is the stator inner radius of the machine.

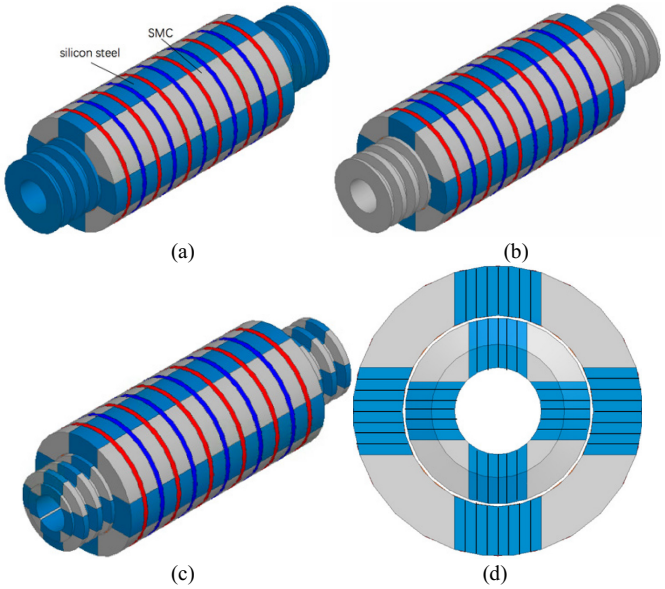

Fig. 7. Main topology of the FSPMTMs with hybrid cores, (a) M3, (b) M4, (c) M5 and (d) axial section diagram of M5.

As shown in Fig. 7(a) (b) (c), there are three machines with the hybrid cores mentioned in this paper. M3 has hybrid stator cores and steel mover, M4 has hybrid stator cores and SMC mover and M5 has hybrid stator and mover. In the hybrid cores, the silicon steels are stacked along the direction shown in Fig. 6(b) and Fig. 7(d), and the other parts are filled by using the SMC cores. Thus, there is no additional eddy current loss resulted, and the proportion of the SMC in hybrid cores can be optimized for achieving best performance according to different rated operation frequency.

After changing the lamination direction of the silicon steel sheet, SMC is preliminarily considered to be used to fill the space with insufficient lamination of the silicon steel sheet. Fig. 8(a) and (b) show the machine structure without SMC. The stacking width W_s of silicon steel sheets are 30 mm and 46 mm respectively. Fig. 9 shows the load thrust waveforms of the three machines, it can be seen that when the SMC core is not filled, the thrust of the machine increases with W_s. When the width of silicon steel is 30 mm, SMC is used to fill the spare part. As can be seen from Fig. 9, average thrust of the machine increases from 264.4 N to 518.5 N. After changing the lamination direction of the silicon steel sheet, the SMC is used to complete the core filling, which is conducive to improving the machine thrust.

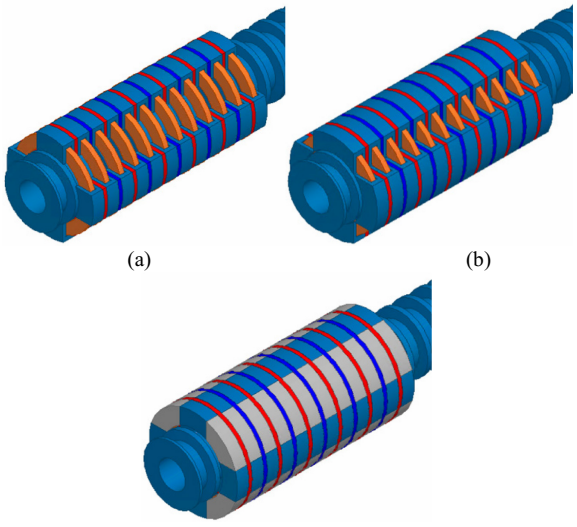

Fig. 8. (a) The stacked width of silicon steel sheet is 30 mm, (b) the stacked width of silicon steel sheet is 46 mm, (c) silicon steel stacked width of 30 mm, the rest of the filling SMC.

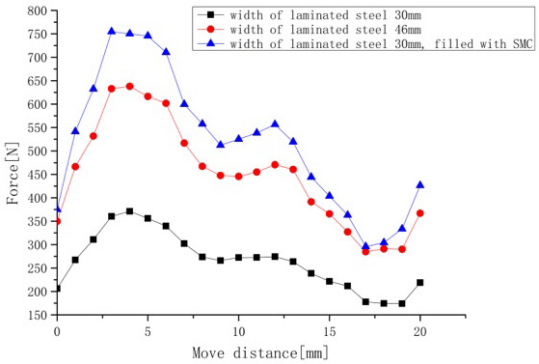

Fig. 9. Thrust in the three cases shown in figure 8.

When the SMC is not filled, the winding is exposed to air and the winding utilization is low. In terms of the amount of PM, when the SMC is not filled, the corresponding permanent magnet in the spare part will also be removed. However, when the SMC is filled, the amount of PM and the magnetic load will be increased and thrust force will be increased. Secondly, the magnetic flux generated by windings can be utilized more effectively when the laminated width of silicon steel sheet is increased or SMC is filled, which will also increase the thrust force.

III. Magnetic Field and Parameter Analysis

After the main dimension is determined, the above five machines are analyzed by using FEM, both PM flux linkage, back EMF, cogging force, thrust, thrust fluctuation and core loss are calculated.

Fig. 10 illustrates the PM flux linkage of these five FSPMTMs. It can be seen that the PM flux linkage of M1 is higher than the others as silicon steels has higher permeability than that of SMC. Thus M2 has lowest PM flux linkage, and it can be concluded that the PM flux linkage can be increased with the used silicon steels increased in M3, M4 and M5. Although the machine M1 has the highest PM flux linkage magnitude, it is not a good machine as the magnetic flux vertically passes through the yoke silicon steel sheet that eddy current is formed and eddy current loss is generated, resulting in severe heating and loss of the machine.

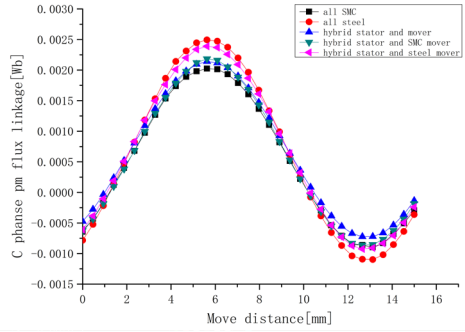

Fig. 10. PM flux linkage of the five FSPMTM.

Fig. 11 illustrates the comparison of back EMF of C phase of these five FSPMTMS at the speed of 2 m/s. It can be found that all the waveforms are sinusoidal, but due to the non-linear magnetic characteristics of the material, the waveform of back EMF has some fluctuations and a certain amount of harmonics.

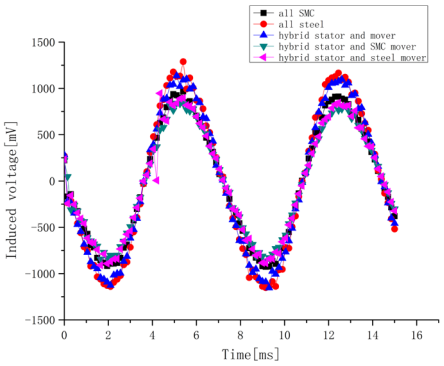

Fig. 11. Induced voltage of the five FSPMTM.

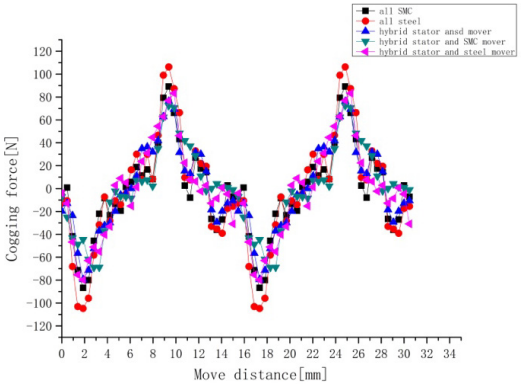

Fig. 12. Cogging force of five FSPMTM with different cores.

In linear machines, cogging force and thrust force are key parameters. As shown in Fig. 12, the cogging forces are different due to the variation of different cores. M1 has the highest cogging force, and its peak-to-peak value reaches to 211.1 N. Compared with the M1, M2 has lower cogging force, reduced from 211.1 N to 175.9 N. M4 proposed in this paper has lowest cogging force, and its peak-to-peak value can be reduced to 141.3 N.

For thrust force comparison in Fig. 13, it can be seen that M1 has the highest average value reaches to 537.4 N and M2 has the lowest average value reaches to 432.6 N. Thrust force of other three machines are in between. For thrust fluctuations, thrust peak-to-peak value of M1 reaches to 238.9 N. Thrust peak-to-peak value of M2 reaches to 226.5 N. For the machines with hybrid cores, thrust peak-to-peak values of M3, M4 and M5 are much smaller, which are 158.9 N, 178.4 N and 135.2 N, respectively. The thrust force of M3, M4 and M5 is between M1 and M2, but the thrust fluctuation is far less than the two.

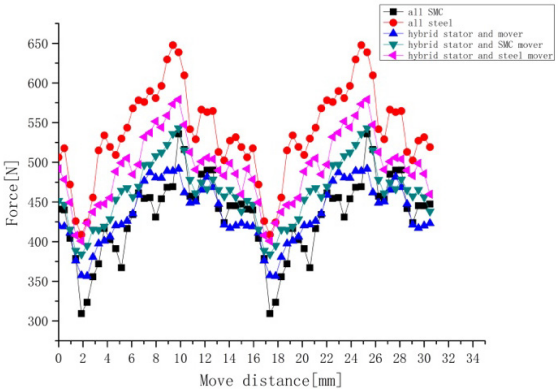

Fig. 13. Thrust force of five FSPMTM with different cores.

The main difference of these machines is the different material combination of stator and mover, and the main difference of loss is the iron loss of stator and mover, in this paper the copper loss, permanent magnet loss, stray loss and mechanical loss are not compared. By using FEM, the alternating core loss of the machine can be calculated by using following formula as:

$$p_{Fe} = K_h f B_m^{\alpha} + K_e \left(f B_m\right)^{\beta} + K_{exc} f^{1.5} B_m^{1.5} \tag{1}$$

α and β are the calculated exponent of hysteresis loss, which is generally considered to be equal to 2 in the calculation of loss. Then the calculation formula of core loss is as follows:

$$p_{Fe} = K_h f B_m^2 + K_e f^2 B_m^2 + K_{exc} f^{1.5} B_m^{1.5} \quad (2)$$

K_h is the hysteresis loss coefficient. K_e is eddy current loss coefficient; K_{exc} is the additional loss coefficient; Corresponding to $K_h f B_m^2$ is the hysteresis loss, $K_e f^2 B_m^2$ is the eddy current loss, $K_{exc} f^{1.5} B_m^{1.5}$ is the additional loss.

In the calculation of core loss, the laminated silicon steel of mover core of M1 and M3 are parallel to the path of flux flow is considered, which means it is different from the actual axial lamination. However, only in this way can the loss calculation formula provided by the software be satisfied, which means that the eddy current loss needs to be calculated separately. When there is more silicon steel in the machine, the core loss is small. As shown in Fig. 14, no load core loss of the five FSPMTMs at a frequency of 140 Hz. M1 has a core loss of 6.812 W and M3 has a core loss of 6.857 W. When the machine contains more SMC materials, its core loss is larger: the core loss of the M2 is 12.528 W and the core loss of M4 is 12.039 W. The core loss of M5 is 9.066 W in the middle position.

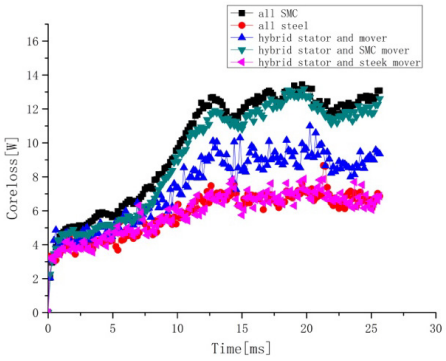

Fig. 14. Core loss comparison of FSPMTFM with different cores under no load condition.

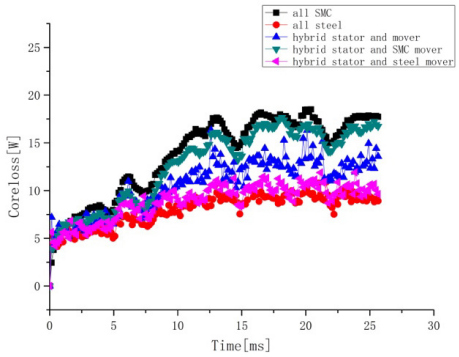

Fig. 15. Core loss comparison of FSPMTFM with different cores at load 140Hz

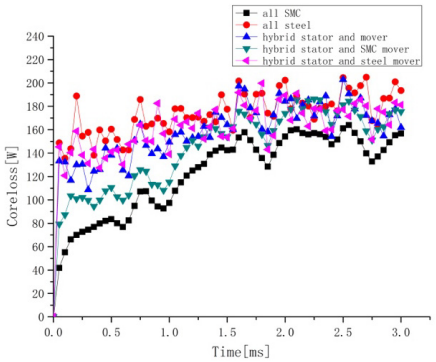

Fig. 16. Core loss comparison of FSPMTFM with different cores at load 1120Hz.

Fig. 15 and Fig. 16 show the load core loss of five FSPMTMs under the move speed of 2 m/s (140 Hz) and 16 m/s (1120 Hz) respectively. As shown in Fig. 15, relationship of each machine's core loss is the same as that of the core when there is no load. For the speed of 2 m/s, the core loss of M2 is the highest one reaches to 17.179 W and the core loss of M1 is the lowest one reaches to 9.338 W. While for the speed of 16 m/s, the core loss of M2 becomes the lowest one reaches to 149.688 W and that core loss of M1 becomes the highest one reaches to 185.031 W. The higher the proportion of SMC used in the machine, the smaller the core loss. It can be seen that in the case of high frequency, the mixed use of SMC in the machine core will greatly improve the machine performance.

In M1, its silicon steel sheets are stacked axially and thus the magnet flux passes vertically through the stator yoke. Fig. 17 shows the radial cross section of a stator core for axial stacked silicon steel sheets. To simplify the calculation, the whole section is divided into 7 regions. From the structure of the machine, regions 1, 2, 3 and 5, 6, 7 are actually symmetric, which reduces the amount of calculation. In the magnetic flux path, regions 3, 4 and 5, namely the yoke and tooth yoke joints of the stator, have magnetic flux passing through the silicon steel sheet vertically, so a large number of eddy current loss is generated. In region 1, 2, 6 and 7, the flux mainly flows along the surface of the silicon steel sheet, and the eddy current loss can be negligible. There are three representative point in region 3, 4 and 5 taken to approximate the change of magnetic density in the region, and each point takes its magnetic density components *Bx*, *By* and *Bz* in the three directions of xyz.

Fig. 17. The radial cross section of the stator of the axial laminated silicon steel sheet.

Fig. 18 shows the variations of the magnet flux density in the stator yoke. As seen, in region 3 and region 5, namely the inflection point of magnetic density flow, there are components in both y and z directions, and the magnetic density component in y direction also reaches nearly 1.0 T. For region 4, the magnetic flux is almost completely along the y direction, and the magnetic density value reaches 1.3 T. Flux density in y direction higher than it in other directions for both the end stator yoke and middle stator yoke. The eddy current loss is proportional to the alternating frequency of the magnetic field, the thickness of the silicon steel sheet and the square of the magnetic flux density, and inversely proportional to the resistivity of the material. However, in the laboratory test, when the magnetic density reaches 0.2 T and the frequency is 50 Hz, the silicon steel sheet will be seriously heated and the

temperature will rise. This is precisely because of the eddy current generated by the magnetic flux passing through the silicon steel sheet vertically, which greatly increases the core loss of the machine. Obviously, this is not allowed. This is exactly the significance of changing the direction of lamination of silicon steel by using hybrid cores mentioned in this paper.

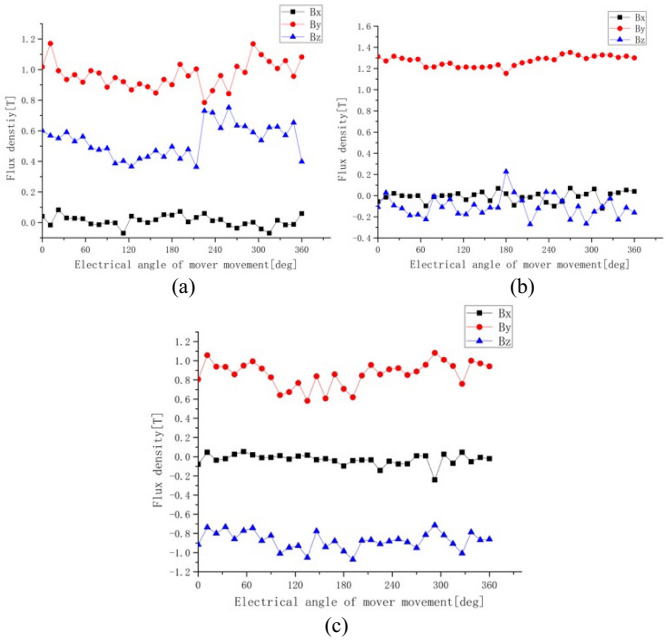

Fig. 18. Variation of magnetic density paths in different regions (a) region 3 (b) region 4 (c) region 5.

IV. End Effect Reduction

Different from the traditional rotary machine, the FSPMTM is opened at two ends, which will destroy the integrity of the magnetic circuit. The end effect can bring the FSPMTM with higher cogging force, higher force ripple and un-symmetry of the PM flux linkage especially when phase A and phase B has the end winding. In this section, a new unequal stator teeth method is proposed for the reduction of end effect. To reduce the calculation load, the 2D FEM is used, and the model is built around the Z-axis, and the software defaults to rotate 360 degrees around the Z-axis. As shown in Fig. 19, the model only shows three stator cores at the end and these three stator cores are labeled as 1, 2, and 3. However in the calculation, there are six stator cores at two ends. The stator width of the end stator cores can be changed from 12 mm-14 mm respectively. In order to make sure that the change of stator width will not affect the volume of the whole machine, the stator and its adjacent PM is determined to be a unit and its overall length needs to be kept unchanged. In this case, there are 27 matches and it has been tabulated in Table II, and W_{s1}, W_{s2}, W_{s3} represents the axial width of the stator core 1, stator core 2 and stator core 3.

As shown in Fig. 20, it is the waveform of A phase PM flux linkage under the combination of different stator and adjacent permanent magnet widths. It can be seen that the waveforms have a wide variation range and each of them has a good sinusoidal property. The phase A is chosen because it contains windings at the end of the stator, and the asymmetry of its PM flux linkage is the most obvious.

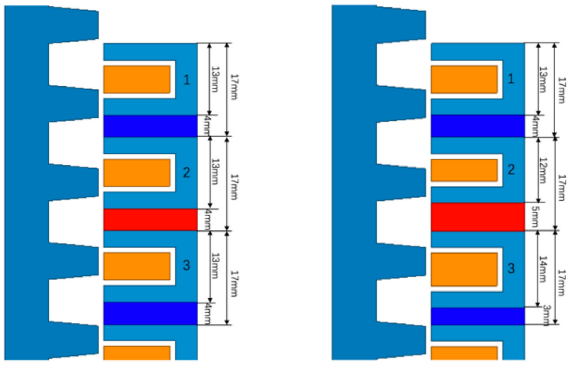

Fig. 19. Topology of the 2-D traditional FSPMTM and optimized FSPMTM. (a) Traditional FSPMTM, (b) optimized FSPMTM.

TABLE II
DIFFERENT STATOR WIDTH MATCHES.

No.	(W_{s1},W_{s2},W_{s3}) /mm	No.	(W_{s1},W_{s2},W_{s3}) /mm	No.	(W_{s1},W_{s2},W_{s3}) /mm
1	(12,12,12)	2	(13,12,12)	3	(14,12,12)
4	(12,13,12)	5	(13,13,12)	6	(14,13,12)
7	(12,14,12)	8	(13,14,12)	9	(14,14,12)
10	(12,12,13)	11	(13,12,13)	12	(14,12,13)
13	(12,13,13)	14	(13,13,13)	15	(14,13,13)
16	(12,14,13)	17	(13,14,13)	18	(14,14,13)
19	(12,12,14)	20	(13,12,14)	21	(14,12,14)
22	(12,13,14)	23	(13,13,14)	24	(14,13,14)
25	(12,14,14)	26	(13,14,14)	27	(14,14,14)

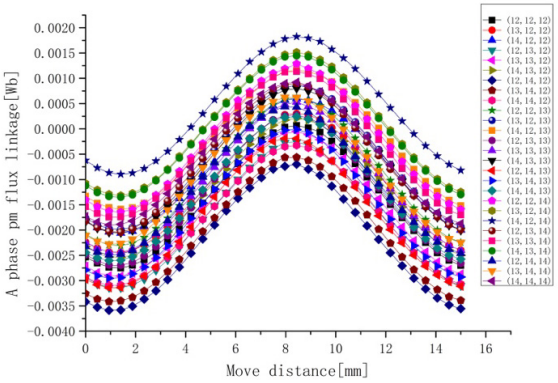

Fig. 20. Waveforms of A phase pm flux linkage with different stator widths.

In order to know the variation of the average value of PM flux linkage under different combinations more intuitively, average value of PM flux linkage under different combinations was made. Fig. 21 shows the average value of all waveforms, ranging from -0.00229 Wb to 0.000371 Wb, and the required PM flux linkage waveform with an average value close to zero. The horizontal coordinate of the figure represents different combination, and each point represents the average value of the permanent magnet flux linkage under this combination.

The effect of the stator width on the PM linkage is different at different positions. The whole waveform can be divided into three stages, each stage is divided into three small parts, each small part is composed of three points. In each small part, as shown in circle 1, under the condition that the widths of No. 2 and No.3 stator remain unchanged, average value of PM flux linkage presents an upward trend with the increase of the width of No. 1 stator. In each stage, as shown in circle 2, is the change in the width of stator No. 2. Under the condition that stator No.1

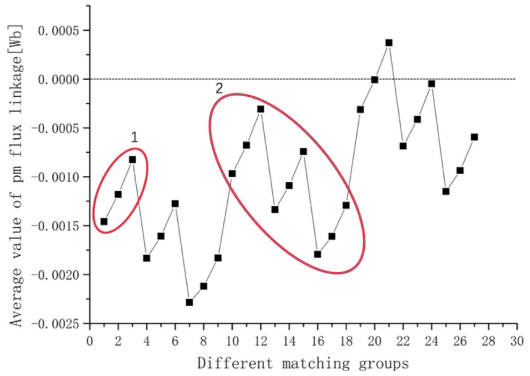

Fig. 21. Average value of A phase pm flux linkage with different stator widths.

and stator No.3 remain unchanged, average value of the PM flux linkage tends to decrease with the increase of the width of stator No.2. For the three stages, under the condition that the widths of stator No.1 and stator No.2 remain unchanged, with the increase of the width of stator No.3, the average value of the PM flux linkage tends to increase.

Fig. 22 shows the average value and peak-to-peak value of PM flux linkage of phase A, it can be seen that the peak-to-peak value of PM flux linkages in phase A do not change a lot while the average value fluctuates greatly with the different un-equal stator width design. The small range of peak-to-peak value will ensure that the thrust does not change a lot.

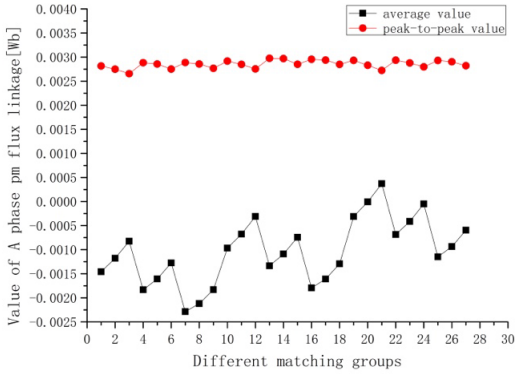

Fig. 22. Peak-to-peak value and average value of A phase pm flux linkage with different stator widths

Fig. 23 shows the comparison of PM flux linkage between the initial design and optimized design. It can be found that the symmetry of PM flux linkage has been improved after the optimization, and the sinusoidal property is not affected.

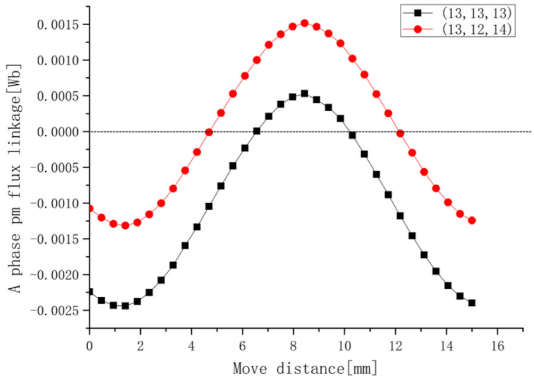

Fig. 23. A phasePM flux linkage before and after optimization.

Fig. 24 and Fig. 25 show the cogging force and thrust force comparison between the initial design and optimized design, it can be seen that the peak-to-peak value of the cogging force and thrust force of the FSPMTM with the optimized design is much lower than that with initial design at the same current density. The peak-to-peak value of cogging force has been reduced from 178 N to 135 N. As well as the average thrust force has been reduced from 519 N to 492 N. However, the force ripple of the initial design is about 0.407 while that for the optimized design is about 0.265. Although the thrust decreased by 4.9%, the peak-to-peak value of thrust decreased by 38.0% from 221.7 N to 131.2 N. The result of induced voltage are both about 1.1V. For the linear drive applications, the low force ripple and quick response are very important, thus the optimized unequal stator width design can bring the FSPMTM better performance.

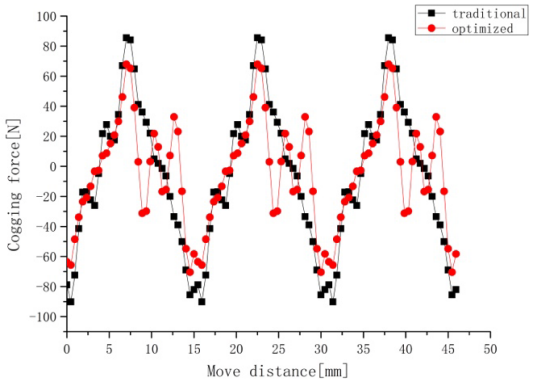

Fig. 24. Cogging force of the traditional FSPMTM and optimized FSPMTM.

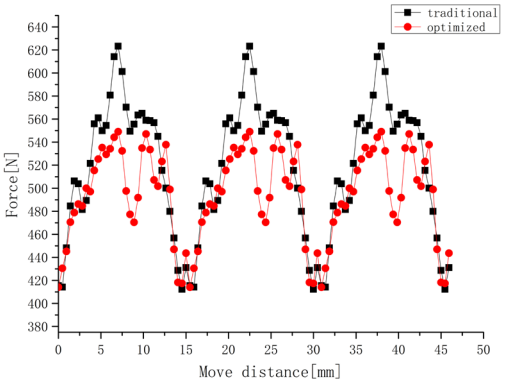

Fig. 25. Thrust force of the traditional FSPMTM and optimized FSPMTM.

For reducing the force ripple and cogging force, the mover skew is another method. In this paper, the mover is divided into 8 parts along the axial direction and each adjacent has been shifted with a determined distance with the others. Fig. 26 shows the mover structure with skewed design.

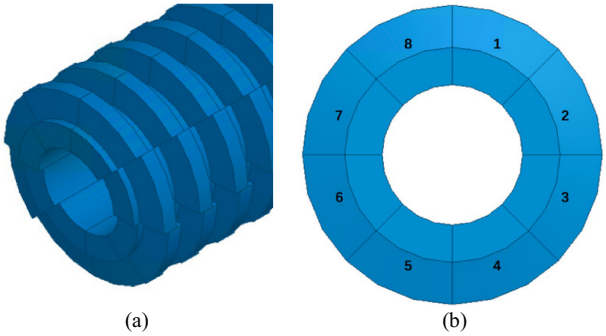

(a) (b)

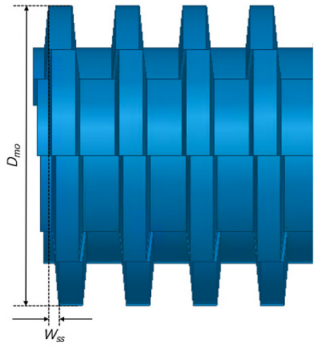

(c)

Fig. 26. (a) Skew slot structure of the mover, (b) axial diagram, (c) radial diagram.

$$\tan\alpha = \frac{W_{ss}}{D_{mo}} \tag{3}$$

$$W_{ss} = D_{mo} * \tan\alpha \tag{4}$$

$$W_{ssn} = W_{ss} / \left(2 / n - 1\right) \tag{5}$$

Where, α is the skew angle of the mover, D_{mo} is the outer diameter of the mover, W_{ss} is the total distance of the skew slot moving in the axial direction, W_{ssn} is the distance of each part of the mover moving in the axial direction, and n is the number of mover that are separated.

Fig. 27 (a) and (b) show the peak-to-peak value of the PM flux linkage and cogging force of the FSPMTM with initial design and optimized unequal stator teeth width with different skew angles. It can be seen that the PM flux linkage will be decreased with the skew angle increases, while for the optimized unequal stator width design its cogging forces decrease quicker than the FSPMTM with initial design.

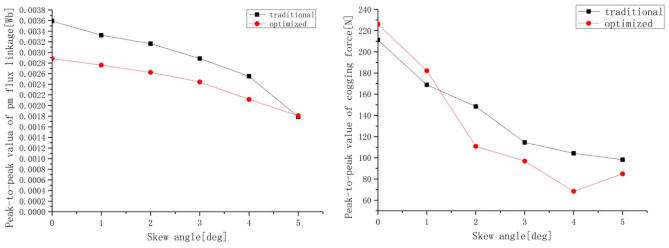

(a) (b)

Fig. 27. (a) Peak-to-peak value of the pm flux linkage, (b) peak-to-peak value of the cogging force.

Fig. 28 shows the cogging force of the optimized FSPMTM in the case of no skew slot and 2deg. The peak-to-peak value of the cogging force of the optimized machine without skew slot reaches 225.9N. The peak-to-peak value of the cogging force of the optimized machine with skew slot angle of 2deg is reduced to 110.8N. This two motors are calculated under steady state, and the running period is the time required by the moving mover to run a tooth slot pitch. Although the mover of optimized motor has skew slot, the tooth slot pitch is the same as the original motor, so the operating frequency is the same.

As shown in Fig. 29, the machine thrust fluctuation after optimization is obviously smaller than that of the original machine. According to the values calculated in software, when the two machines are of the same thrust, the peak-to-peak value

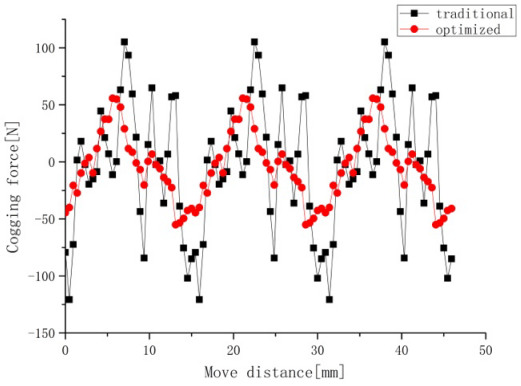

Fig. 28. Cogging force of the FSPMTM in traditional and optimized skew angle.

of the original machine's thrust is 177.5 N, while the thrust fluctuation of the optimized machine is only 107.6 N, which reduces by 39.4%, and the fluctuation ratio is 0.35 and 0.21, respectively. Thus in the new structure, the machine can be more stable operation.

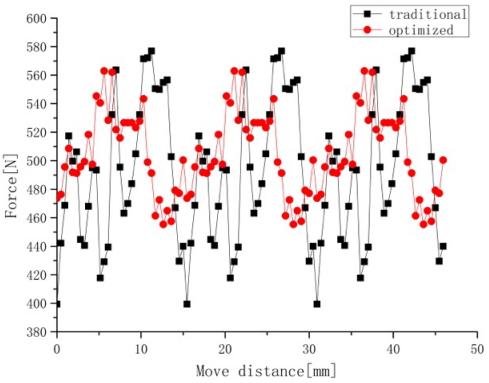

Fig. 29. Thrust of the FSPMTM in traditional and optimized skew angle.

V. Conclusion

In this paper, FSPMTM with hybrid cores is proposed, designed and analyzed. By using SMC material, the stack direction of silicon steel sheet can be changed, and the eddy current loss has been greatly reduced. To ensure the thrust of the machine does not decrease too much, increase the amount of the silicon steel sheet at low frequency and increase the amount of SMC at high frequency.

Although M1 has the largest thrust force, it has the largest thrust fluctuation and eddy current loss as well. At the same time, the hysteresis loss of M2 at low frequency is also large, and the thrust is small. After using the hybrid cores, M3, M4 and M5 firstly avoid a large amount of eddy current loss caused by the silicon steel sheet, and secondly, the thrust fluctuation is greatly reduced. M4's average thrust is 6.7% higher and the thrust fluctuation is 29.8% lower than M2, and the core loss is lower at low frequency. Compared with M1, although the average thrust decreased by 14.1%, but the thrust fluctuation decreased by 33.5%. This result is beneficial to reduce the thrust fluctuation of the machine and make it work smoothly, and the core loss is lower in the case of high frequency. The differences of machines' core loss at different frequencies show that the hybrid cores and the lamination mode of silicon steel sheet presented in this paper can effectively reduce the core loss

of the machine at different operating frequencies.

In order to reduce the impact of the end effect, the unequal width stator is proposed. On the premise of not changing the volume of machine and the amount of each material, the end effect is weakened. Moreover, the cogging force and thrust fluctuation caused by end effect is reduced by using the unequal width stator to adjust the symmetry of the permanent magnet flux linkage and mover skew slot. This design method provides a way to reduce the cogging force and thrust fluctuation of the FSPMTM.

REFERENCE

[1] B. Zhang, M. Cheng, J, Wang, and S. Zhu, "Optimization and analysis of a yokeless linear flux switching permanent magnet machine with high thrust density," *IEEE Trans. Magn*., vol. 51, no. 11, pp. 8204804, Nov.2015

[2] R. Cao, M. Cheng, C. Mi, W. Hua, X. Wang, and W. Zhao, "Modeling of a complementary and modular linear flux-switching permanent magnet machine for urban rail transit applications," *IEEE Trans. Energy Convers*., vol. 27, no. 2, pp. 489-497, Jun. 2012.

[3] J. F. Eastham, "Novel synchronous machines: Linear and disc," *Inst. Electr. Eng. Proc.—B*, vol. 137, no. 1, pp. 49–58, 1990.

[4] A. W. Van Zyl, C. G. Jeans, R. J. Cruise, and C. F. Landy, "Comparison of force to weight ratios between a single-sided linear synchronous machine and a tubular linear synchronous machine," in *Proc. IEEE Int. Electr. Mach. Drives Conf*., Seattle, WA, 1999, pp. 571–573.

[5] J. Chang, D. Kang, J. Lee, and J. Hong. "Development of transverse flux linear machine with permanent-magnet excitation for direct drive applications," *IEEE Trans. Magn*., vol. 41, no. 5, pp. 1936-1939, May. 2005.

[6] Wang Jiabin, Wang Weiya, Kais Atallah, et al. "Design Considerations for Tubular Flux-Switching Permanent Magnet Machines," *IEEE Trans. Magn*., vol. 44, no. 11, pp. 4026-4032, Nov. 2008.

[7] Liang Yan, Wei Li, Zongxia Jiao, Chin-Yin Chen, and Ming Chen, "Design and Modeling of Three-phase Tubular Linear Flux-Switching Permanent Magnet Machine," in *Proceedings of 2014 IEEE Chinese Guidance, Navigation and Control Conference*, August 8-10, 2014, Yantai, China.

[8] Chengcheng Liu, Shaopeng Wang, Youhua Wang, Gang Lei, Youguang Guo, and Jianguo Zhu, "Development of a New Flux Switching Transverse Flux Machine with the Ability of Linear Motion," *CES Transactions on Electrical Machines and Systems*., vol. 2, no. 3, pp. 384-391, 2018.

[9] Y. G. Guo, J. G. Zhu, H. Y. Lu, Y. J. Li, and J. X. Jin, "Core Loss Computation in a Permanent Magnet Transverse Flux Machine with Rotating Fluxes," *IEEE Trans. Magn*., vol. 50, no. 11, Nov 2014.

[10] Xuzhen Huang, Qiang Tan, XiaoJing Xue, "Calculation and Analysis of the Loss for Tubular Flux-switching Permanent Magnet Linear Machine," in *Proceedings of 2014 17th International Conference on Electrical Machines and Systems (ICEMS)*, Oct. 22-25, 2014, Hangzhou, China.

[11] Ahmed M. Mohammed, Michael Galea, Tom Cox, Chris Gerada, "Consideration on Eddy Current Reduction Techniques for Solid Materials Used in Unconventional Magnetic Circuits," *IEEE Trans. Ind. Electronics*, vol. 66, no. 6, pp. 4870-4879, 2019.

[12] N. Bianchi, S. Bolognani, D. Corte, and F. Tonel, "Tubular linear permanent magnet machines: An overall comparison," *IEEE Trans. Ind. Appl*., vol. 39, no. 2, pp. 466–475, 2003.

[13] Wang Canfei, Shen Jianxin, W. Yu, et al. "A New Method for Reduction of Detent Force in Permanent Magnet Flux-Switching Linear Machines," *IEEE Trans. Magn*., vol. 45, no. 6, pp. 2843-2846.

[14] Ji Jinghua, Yan Shujun, Zhao Wenxiang, et al. "Minimization of Cogging Force in a Novel Linear Permanent-Magnet Machine for Artificial Hearts," *IEEE Trans. Magn*., vol. 45, no. 6, July 2013.

[15] C. C. Liu, Y. H. Wang, G. Lei, Y. G. Guo, and J. G. Zhu, "Design and analysis of a 3D-flux flux-switching permanent magnet machine with SMC cores and ferrite magnets," *AIP Advances* 7, 056632 (2017); doi: 10.1063/1.4974524.

[16] Y. Wang, et al., "Cogging torque reduction in permanent magnet flux-switching machines by rotor teeth axial pairing," *IET Electric Power Applications*., vol. 4, no.8, pp. 500-506, 2010.

[17] Z. Q. Zhu, A. S. Thomas, J. T. Chen and G. W. Jewell, "Cogging torque in flux-switching permanent magnet machines," *IEEE Trans. Magn*., vol. 45, no. 10, pp. 4708–4711, Oct. 2009.

[18] W. J. Hao and Y. Wang, "Comparison of the Stator Step Skewed Structures for Cogging Force Reduction of Linear Flux Switching Permanent Magnet Machines" *Energies,* vol. 11, no. 8, pp. 1-14, 2018.

[19] Inoue. M and Sato K, "An approach to a suitable stator length for minimizing the detent force of permanent magnet linear synchronous machines," *IEEE Trans. Magn*., vol. 36, no. 4, pp. 1890–1893, 2000.

[20] Fei Weizhong, Patrick Chi Kwong Luk and Shen Jianxin. "Torque analysis of permanent-magnet flux switching machines with rotor step skewing," *IEEE Trans. Magn*., vol. 48, no. 10, pp. 2664–2673, 2012.

Shaopeng Wang was born in Hebei, China, in 1993. He received the B.E. degree in Electrical Engineering from Hebei University of Technology, Tianjin, China, in 2016, where he is currently working toward the M.E. degree.

His current research interests include design and optimization of electromagnetic devices.

Chengcheng Liu (S'14 – M'16) was born in Jiangsu, China in 1988. He received the B.E. degree in automation engineering from Yangzhou University, Yangzhou, China, in 2010 and the Ph.D. degree in electrical engineering from Hebei University of Technology, Tianjin, China, in 2016. He was a joint Ph.D. student supported by Chinese scholarship council in the University of Technology, Sydney, Australia.

He is currently a Lecturer of Hebei University of Technology, Tianjin China. His research interests include the design, analysis, control and optimization of electromagnetic devices.

Youhua Wang received the B.E. degree from Xian Jiaotong University, Xian, China, in 1987; the M.E. degree from the Hebei University of Technology, Tianjin, China, in 1990; and the Ph.D. from Fuzhou University, Fuzhou, China, in 1994, all in electrical apparatus.

He is currently a Professor at the College of Electrical Engineering. His currently research interests include measurement and modeling of properties of magnetic materials, numerical analysis of the electromagnetic field, and electromagnetic device design, analysis and optimization.

Gang Lei (M'14)received the B.S. degree in mathematics from Huanggang Normal University, Huanggang, China, in 2003, and the M.S. degree in mathematics and the Ph.D. degree in electrical engineering from Huazhong University of Science and Technology, Wuhan, China, in 2006 and 2009 respectively.

He is currently a Lecturer at the at the School of Electrical and Data Engineering University of Technology Sydney, NSW, Australia. His current research interests include electromagnetic inverse problems, design optimization of electrical drive systems and renewable energy systems.

Youguang Guo (S'02 - M'05 – SM'06) received the B.E. degree from Huazhong University of Science and Technology, Wuhan, China, in 1985; the M.E. degree from the Zhejiang University, Zhejiang, China, in 1988; and the Ph.D. degree from the University of Technology, Sydney (UTS), NSW, Australia, in 2004, all in electrical engineering.

He is currently an Associate Professor at the School of Electrical and Data Engineering, University of Technology Sydney, UTS. His research fields include measurement and modeling of properties of magnetic materials, numerical analysis of the electromagnetic field, electrical machine design optimization, and power electronics drives and control.

Jianguo Zhu (S'90 – M'96 – SM'03) received the B.E. degree from Jiangsu Institute of Technology, Zhenjiang, China, in 1982; the M.E. degree from the Shanghai University of Technology, Shanghai, China, in 1987; and the Ph.D. degree from the University of Technology, Sydney (UTS), NSW, Australia, in 1995, all in electrical engineering.

He is currently a Professor of Electrical Engineering and the Head at the School of electrical and information engineering, University of Sydeny. His current research interests include electromagnetic, magnetic properties of materials, electrical machines, and drives, power electronics, and green energy systems.